J. Wind Eng. Ind. Aerodyn. 97 (2009) 573–580

Contents lists available at ScienceDirect

Journal of Wind Engineering and Industrial Aerodynamics

journal homepage: www.elsevier.com/locate/jweia

An approximation method for resonant response with coupling modes of structures under wind action

Ming Gu *, Xuan-yi Zhou

State Key Laboratory of Disaster Reduction in Civil Engineering, Tongji University, Siping Road 1239, Shanghai 200092, China

ARTICLE INFO

Article history:
Received 15 March 2006
Received in revised form
31 May 2009
Accepted 21 August 2009
Available online 25 September 2009

Keywords:
Flexible structure
Resonant response
Mode coupling factor
Modified SRSS method

ABSTRACT

Effects of multi-mode coupling should be taken into account in computing the resonant buffeting response of some kinds of flexible structures with low damping and concentrated modes. In this paper, a new concept of "mode coupling factor" for computation of coupling effects between multi-mode resonant responses of the structures is proposed. On the base of the mode coupling factor, a modified SRSS method for computation of the resonant response contributed by multi-modes and their coupling effects of the structures is further raised. The roof structure of Shanghai Southern Railway Station is then taken as the case study to indicate the application and to verify the precision of the mode coupling factor and the modified SRSS method. The computaion results indicate that the mode coupling factor can quantitatively describe the contribution of mode coupling to the resonant response; and the modified SRSS method can make the computation of structural resonant response with consideration of mode coupling effects simpler.

1. Introduction

Wind loads acting on large roof structures are usually key factors for the structural design. Different from tall buildings, large-span roof structures have concentrated modes, and thus multi-mode responses and their coupling effects should be considered in the computation of dynamic response and of equivalent static wind loads (Nakamura et al., 1994; Uematsu et al., 1999, 2001).

Davenport (1995) proposed a basic idea that wind induced response of a building could be divided into mean, background and resonant response components, which have been adopted in follow-up researchers and structural load codes in different countries to compute the wind induced responses of structures. LRC method (Kasperski and Niemann, 1992) has been suggested for computations of the background response component of tall buildings and large roof structures (Zhou et al., 1999, 2000; Holmes and Kasperski, 1996; Holmes, 1999, 2002). As for the resonant response component of tall buildings, the total response could approximately be regarded as the contribution only from the fundamental mode response (Zhou et al., 1999, 2000). While for large-span roofs, higher mode responses should be considered. A new method composed of LRC method and inertial wind load method was recently proposed by Holmes to compute the equivalent static wind loads acting on roofs (Holmes and Kasperski, 1996; Holmes, 2002). In this method multi-modal response contribution was taken into account but the coupling effect between the modes was not considered. In fact, for some roofs with higher fundamental frequency, the background response may play a dominant role in the total response; while for those with lower fundamental frequency, resonant response may also be important and the coupling effects between modes should not be negligible (Gu et al., 2002, 2003).

This paper thus derives a new mode coupling factor to describe the multi-mode coupling effect between modal resonant responses. An approximate and practical method named modified SRSS method (hereafter referred to as MSRSS method) for computation of wind induced resonant response with consideration of the mode coupling effect is accordingly developed. This method might be useful for developing a practical method for equivalent static wind loads on structures taking mode coupling effects into account. A real roof structure is finally taken as the case example to show the application and to verify the precision of the mode coupling factor and the MSRSS method.

2. Mode coupling factor and MSRSS method

2.1. Approximate formulation for resonant response with mode coupling

The equation governing the motion of a structure under the action of turbulent wind can be written in the matrix style as

$$[M]\{\ddot{y}\}+[C]\{\dot{y}\}+[K]\{y\}=[R]\{p(t)\} \quad (1)$$

* Corresponding author. Tel./fax: +86 21 65981210.
E-mail address: minggu@mail.tongji.edu.cn (M. Gu).

0167-6105/$ - see front matter © 2009 Elsevier Ltd. All rights reserved.
doi:10.1016/j.jweia.2009.08.013

where [M], [C] and [K] are the mass, damping and stiffness matrixes, respectively; $\{y\}$, $\{\dot{y}\}$ and $\{\ddot{y}\}$ are the displacement, velocity and acceleration vectors of the structure, respectively; [R] is the force indicating matrix (m-by-n matrix) composed of zero and unity, which expands the force vector $\{p(t)\}$ of m dimension into the vector of n dimension.

Based on the random vibration theory and the hypothesis of classic damping, the power spectrum density (PSD in short) of dynamic displacement of the structure, which can take into account of the coupling effects between modes, can be written as

$$[S_{yy}(\omega)] = \sum_{j=1}^{n}\sum_{k=1}^{n}\{\phi_j\}H_j^*(i\omega)\{\phi_j\}^T[R][S_{pp}(\omega)][R]^T\{\phi_k\}H_k(i\omega)\{\phi_k\}^T \tag{2}$$

that is,

$$[S_{yy}(\omega)] = \sum_{j=1}^{n}\sum_{k=1}^{n}\{\phi_j\}H_j^*(i\omega)[S_{FF}(\omega)]H_k(i\omega)\{\phi_k\}^T \tag{3}$$

where $\{\phi_j\}$ is the jth modal shape; $H_j(i\omega)$ is the jth frequency response function; $[S_{FF}(\omega)]$ the matrix of generalized wind forces; and n is the number of modes participating in the vibration.

In real applications, some important responses, i.e., dynamic displacements and internal forces, of major structural members, should be obtained for structural design. The PSD of ith displacement response (i=1,2,3…,m; m is the total number of the concerned displacement responses for structural design. For the simplification of expression, the 'ith response' is hereafter referred to as "response") can be written as follows:

$$S_{ii}(\omega) = \sum_{j=1}^{n}\sum_{k=1}^{n}\phi_{ij}H_j^*(i\omega)S_{F_jF_k}(\omega)H_k(i\omega)\phi_{ik} \tag{4}$$

Integrating Eq. (4) with respect to ω over [ω_l, ω_h], where ω_l and ω_h are the lower limit and upper limit including the concerned resonant frequencies for the integration, one can obtain the variance of resonant dynamic displacement. The resonant displacement includes the coupling effects between modes and is regarded as the precise response in the paper for comparison later on.

If the real part and imaginary part in Eq. (4) are notated by Re[] and Im[], respectively, Eq. (4) can be re-written as

$$\begin{aligned} S_{ii}(\omega) &= \sum_{j=1}^{n}\sum_{k=1}^{n}\phi_{ij}\phi_{ik}\{\mathrm{Re}[H_j^*(i\omega)H_k(i\omega)] + \mathrm{Im}[H_j^*(i\omega)H_k(i\omega)]i\}S_{F_jF_k} \\ &= \sum_{j=1}^{n}\sum_{k=1}^{n}\phi_{ij}\phi_{ik}\mathrm{Re}[H_j^*(i\omega)H_k(i\omega)]S_{F_jF_k} \\ &\quad + \sum_{j=1}^{n}\sum_{k=1}^{n}\phi_{ij}\phi_{ik}\mathrm{Im}[H_j^*(i\omega)H_k(i\omega)]iS_{F_jF_k} \end{aligned} \tag{5}$$

Vanmarcke has derived the expression of $\mathrm{Re}[H_j^*(i\omega)H_k(i\omega)]$ (Vanmarcke, 1972) as,

$$\begin{aligned} \mathrm{Re}[H_j^*(i\omega)H_k(i\omega)] &= \tfrac{1}{2}[NN_{kj} \\ &\quad - PP_{kj}(1-\omega_k^2/\omega^2)]|H_k(i\omega)|^2 + \tfrac{1}{2}[NN_{jk} \\ &\quad - PP_{jk}(1-\omega_j^2/\omega^2)]|H_j(i\omega)|^2 \end{aligned} \tag{6}$$

where NN_{jk} and PP_{jk} are both relative to the jth structural damping ratio ζ_j, kth damping ratio ζ_k and q; $q=\omega_k/\omega_j$; ω_k and ω_j are the kth and the jth natural frequencies, respectively. The formulas for NN_{jk} and PP_{jk}, which have been given by Vanmarcke (1972), are

$$NN_{jk} = \frac{1}{D_{jk}}\left\{8q\zeta_j(\zeta_k+\zeta_j q)[(1-q^2)^2 - 4q(\zeta_j-\zeta_k q)(\zeta_k-\zeta_j q)]\right\} \tag{7}$$

$$PP_{jk} = \frac{1}{D_{jk}}\left\{2(1-q^2)[4q(\zeta_j-\zeta_k q)(\zeta_k-\zeta_j q) - (1-q^2)^2]\right\} \tag{8}$$

where

$$D_{jk} = 8q^2[(\zeta_j^2+\zeta_k^2)(1-q^2)^2 - 2(\zeta_k^2-\zeta_j^2q^2)(\zeta_j^2-\zeta_k^2q^2)] + (1-q^2)^4 \tag{9}$$

Let

$$T_{jk} = \frac{1}{2}[NN_{jk} - PP_{jk}(1-\omega_j^2/\omega^2)]|H_j(i\omega)|^2 \tag{10}$$

Combining Eqs. (6) and (10) leads to

$$\begin{aligned} &\sum_{j=1}^{n}\sum_{k=1}^{n}\phi_{ij}\phi_{ik}\mathrm{Re}[H_j^*(i\omega)H_k(i\omega)]S_{F_jF_k} = \sum_{j=1}^{n}\sum_{k=1}^{n}\phi_{ij}\phi_{ik}(T_{kj}+T_{jk})S_{F_jF_k} \\ &= \sum_{j=1}^{n}\sum_{k=1}^{n}\phi_{ij}\phi_{ik}T_{kj}S_{F_jF_k} + \sum_{j=1}^{n}\sum_{k=1}^{n}\phi_{ij}\phi_{ik}T_{jk}S_{F_jF_k} \end{aligned} \tag{11}$$

Furthermore, $\sum_{j=1}^{n}\sum_{k=1}^{n}\phi_{ij}\phi_{ik}T_{kj}S_{F_jF_k}$ can be approximated by $\sum_{k=1}^{n}\sum_{j=1}^{n}\phi_{ik}\phi_{ij}T_{jk}S_{F_kF_j}$, that is,

$$\sum_{j=1}^{n}\sum_{k=1}^{n}\phi_{ij}\phi_{ik}T_{kj}S_{F_jF_k} \approx \sum_{k=1}^{n}\sum_{j=1}^{n}\phi_{ik}\phi_{ij}T_{jk}S_{F_kF_j} = \sum_{j=1}^{n}\sum_{k=1}^{n}\phi_{ik}\phi_{ij}T_{jk}S_{F_kF_j}, \tag{12}$$

This approximation may only lead to a very small error to the final computation result of structural dynamic response, which will be illustrated in the following case study. In fact, in the atmosphere boundary layer it appears that the ratio of imaginary part to real part of the cross-spectral density of wind force acting on structures is small (Simu and Scanlan, 1996). Even so, the imaginary part of the cross-spectral density of the force is taken into account in the following analysis. Thus one can derive the following equation:

$$\begin{aligned} &\sum_{j=1}^{n}\sum_{k=1}^{n}\phi_{ij}\phi_{ik}T_{kj}S_{F_jF_k} + \sum_{j=1}^{n}\sum_{k=1}^{n}\phi_{ij}\phi_{ik}T_{jk}S_{F_jF_k} = \sum_{j=1}^{n}\sum_{k=1}^{n}\phi_{ik}\phi_{ij}T_{jk}S_{F_kF_j} \\ &+ \sum_{j=1}^{n}\sum_{k=1}^{n}\phi_{ij}\phi_{ik}T_{jk}S_{F_jF_k} = \sum_{j=1}^{n}\sum_{k=1}^{n}\phi_{ik}\phi_{ij}T_{jk}(S_{F_kF_j}+S_{F_jF_k}) \\ &= \sum_{j=1}^{n}\sum_{k=1}^{n}\phi_{ik}\phi_{ij}T_{jk}2\,\mathrm{Re}(S_{F_jF_k}) \end{aligned} \tag{13}$$

In the last derivation step in the above equation, the property of Hermite matrix is applied. Therefore, the first term on the right hand in Eq. (5) can be written as follows:

$$\begin{aligned} &\sum_{j=1}^{n}\sum_{k=1}^{n}\phi_{ij}\phi_{ik}\mathrm{Re}[H_j^*(i\omega)H_k(i\omega)]S_{F_jF_k} \\ &= \sum_{j=1}^{n}\sum_{k=1}^{n}\phi_{ik}\phi_{ij}NN_{jk}|H_j(i\omega)|^2\mathrm{Re}(S_{F_jF_k}) \\ &+ \sum_{j=1}^{n}\sum_{k=1}^{n}\phi_{ik}\phi_{ij}PP_{jk}(1-\omega_j^2/\omega^2)|H_j(i\omega)|^2\mathrm{Re}(S_{F_jF_k}) \end{aligned} \tag{14}$$

As for the imaginary part of $[H_j^*(i\omega)H_k(i\omega)]$, Vanmarcke (1972) gave

$$\begin{aligned} \mathrm{Im}[H_j^*(i\omega)H_k(i\omega)] &= 2\left\{\left[VV_{kj}\left(\frac{\omega}{\omega_k}\right) + WW_{kj}\left(\frac{\omega}{\omega_k}\right)^3\right]|H_k(i\omega)|^2\right. \\ &\quad \left. - \left[VV_{jk}\left(\frac{\omega}{\omega_j}\right) + WW_{jk}\left(\frac{\omega}{\omega_j}\right)^3\right]|H_j(i\omega)|^2\right\} \end{aligned} \tag{15}$$

where VV_{jk} and WW_{jk} are the function of the structural natural frequencies, ω_j and ω_k, and damping ratios, ζ_j and ζ_k, and $q=\omega_k/\omega_j$;

$$VV_{jk}=\frac{1}{Q_{jk}}\{q(\zeta_k-\zeta_j q)[\zeta_j(\zeta_j-\zeta_k q^2)-(1-q^4)]-(\zeta_j-\zeta_k q)(\zeta_j-\zeta_k q^2)\} \tag{16}$$

$$WW_{jk}=\frac{1}{Q_{jk}}[q(\zeta_k-\zeta_j q)(\zeta_j-\zeta_k q^2)+(\zeta_j-\zeta_k q)(q^4-1)] \tag{17}$$

and

$$Q_{jk}=q^4(\zeta_j^2+\zeta_k^2)-\zeta_j\zeta_k q^2(1+q^4)+(1-q^4)^2 \tag{18}$$

Letting

$$U_{jk}=2\left[VV_{jk}\left(\frac{\omega}{\omega_j}\right)+WW_{jk}\left(\frac{\omega}{\omega_j}\right)^3\right]|H_j(i\omega)|^2 \tag{19}$$

and combining Eqs. (15) and (19) leads to

$$\sum_{j=1}^{n}\sum_{k=1}^{n}\phi_{ij}\phi_{ik}\mathrm{Im}[H_j^*(i\omega)H_k(i\omega)]iS_{F_jF_k}=\sum_{j=1}^{n}\sum_{k=1}^{n}\phi_{ij}\phi_{ik}(U_{kj}-U_{jk})iS_{F_jF_k}=\sum_{j=1}^{n}\sum_{k=1}^{n}\phi_{ij}\phi_{ik}U_{kj}iS_{F_jF_k}-\sum_{j=1}^{n}\sum_{k=1}^{n}\phi_{ij}\phi_{ik}U_{jk}iS_{F_jF_k} \tag{20}$$

Further considering

$$\sum_{j=1}^{n}\sum_{k=1}^{n}\phi_{ij}\phi_{ik}U_{kj}iS_{F_jF_k}=\sum_{k=1}^{n}\sum_{j=1}^{n}\phi_{ik}\phi_{ij}U_{jk}iS_{F_kF_j}=\sum_{j=1}^{n}\sum_{k=1}^{n}\phi_{ik}\phi_{ij}U_{jk}iS_{F_kF_j} \tag{21}$$

the following equation can be derived:

$$\begin{aligned}&\sum_{j=1}^{n}\sum_{k=1}^{n}\phi_{ij}\phi_{ik}U_{kj}iS_{F_jF_k}-\sum_{j=1}^{n}\sum_{k=1}^{n}\phi_{ij}\phi_{ik}U_{jk}iS_{F_jF_k}\\&=\sum_{j=1}^{n}\sum_{k=1}^{n}\phi_{ik}\phi_{ij}U_{jk}iS_{F_kF_j}-\sum_{j=1}^{n}\sum_{k=1}^{n}\phi_{ij}\phi_{ik}U_{jk}iS_{F_jF_k}\\&=\sum_{j=1}^{n}\sum_{k=1}^{n}\phi_{ij}\phi_{ik}U_{jk}i(S_{F_kF_j}-S_{F_jF_k})\\&=\sum_{j=1}^{n}\sum_{k=1}^{n}\phi_{ij}\phi_{ik}U_{jk}i[-2\,\mathrm{Im}(S_{F_jF_k})i]\\&=\sum_{j=1}^{n}\sum_{k=1}^{n}\phi_{ij}\phi_{ik}U_{jk}2\,\mathrm{Im}(S_{F_jF_k})\end{aligned} \tag{22}$$

Substituting Eq. (19) into Eq. (22) leads to

$$\begin{aligned}&\sum_{j=1}^{n}\sum_{k=1}^{n}\phi_{ij}\phi_{ik}\,\mathrm{Im}[H_j^*(i\omega)H_k(i\omega)]iS_{F_jF_k}\\&=\sum_{j=1}^{n}\sum_{k=1}^{n}\phi_{ij}\phi_{ik}4VV_{jk}\left(\frac{\omega}{\omega_j}\right)|H_j(i\omega)|^2\,\mathrm{Im}(S_{F_jF_k})+\sum_{j=1}^{n}\sum_{k=1}^{n}\phi_{ij}\phi_{ik}4WW_{jk}\left(\frac{\omega}{\omega_j}\right)^3|H_j(i\omega)|^2\,\mathrm{Im}(S_{F_jF_k})\end{aligned} \tag{23}$$

Combining Eqs. (14) and (23), one can derive formula of the power spectrum of dynamic displacement as follows:

$$\begin{aligned}S_{ii}(\omega)&=\sum_{j=1}^{n}\sum_{k=1}^{n}\phi_{ij}\phi_{ik}\,\mathrm{Re}[H_j^*(i\omega)H_k(i\omega)]S_{F_jF_k}+\sum_{j=1}^{n}\sum_{k=1}^{n}\phi_{ij}\phi_{ik}\,\mathrm{Im}[H_j^*(i\omega)H_k(i\omega)]iS_{F_jF_k}\\&=\sum_{j=1}^{n}\sum_{k=1}^{n}\phi_{ik}\phi_{ij}NN_{jk}|H_j(i\omega)|^2\,\mathrm{Re}(S_{F_jF_k})+\sum_{j=1}^{n}\sum_{k=1}^{n}\phi_{ik}\phi_{ij}PP_{jk}(1-\omega_j^2/\omega^2)|H_j(i\omega)|^2\,\mathrm{Re}(S_{F_jF_k})\\&\quad+\sum_{j=1}^{n}\sum_{k=1}^{n}\phi_{ij}\phi_{ik}4VV_{jk}\left(\frac{\omega}{\omega_j}\right)|H_j(i\omega)|^2\,\mathrm{Im}(S_{F_jF_k})+\sum_{j=1}^{n}\sum_{k=1}^{n}\phi_{ij}\phi_{ik}4WW_{jk}\left(\frac{\omega}{\omega_j}\right)^3|H_j(i\omega)|^2\,\mathrm{Im}(S_{F_jF_k})\end{aligned} \tag{24}$$

Integrating Eq. (24) with respect to ω over $[\omega_{j,s},\omega_{j,e}]$, where the jth mode resonant frequency range $[\omega_{j,s},\omega_{j,e}]$ (j=1,2,…,n) is a narrow frequency band for structures with low damping, can lead to the variance of the resonant displacement response as

$$\begin{aligned}\sigma_{R,i}^2&=\int_{\omega_{R,s}}^{\omega_{R,e}}S_{ii}(\omega)\,d\omega\\&=\sum_{j=1}^{n}\sum_{k=1}^{n}\phi_{ik}\phi_{ij}NN_{jk}\int_{\omega_{j,s}}^{\omega_{j,e}}|H_j(i\omega)|^2\,\mathrm{Re}(S_{F_jF_k}(\omega))\,d\omega\\&\quad+\sum_{j=1}^{n}\sum_{k=1}^{n}\phi_{ik}\phi_{ij}PP_{jk}\int_{\omega_{j,s}}^{\omega_{j,e}}(1-\omega_j^2/\omega^2)|H_j(i\omega)|^2\,\mathrm{Re}(S_{F_jF_k}(\omega))\,d\omega\\&\quad+\sum_{j=1}^{n}\sum_{k=1}^{n}\phi_{ik}\phi_{ij}4VV_{jk}\int_{\omega_{j,s}}^{\omega_{j,e}}\left(\frac{\omega}{\omega_j}\right)|H_j(i\omega)|^2\,\mathrm{Im}(S_{F_jF_k}(\omega))\,d\omega\\&\quad+\sum_{j=1}^{n}\sum_{k=1}^{n}\phi_{ik}\phi_{ij}4WW_{jk}\int_{\omega_{j,s}}^{\omega_{j,e}}\left(\frac{\omega}{\omega_j}\right)^3|H_j(i\omega)|^2\,\mathrm{Im}(S_{F_jF_k}(\omega))\,d\omega\end{aligned} \tag{25}$$

In fact,

$$\sigma_{R,ji}^2=\phi_{ij}^2\int_{\omega_{j,s}}^{\omega_{j,e}}|H_j(i\omega)|^2\,\mathrm{Re}(S_{F_jF_j})\,d\omega$$

is the variance of the jth modal resonant displacement excluding the coupling terms between modes. Due to $PP_{jk}=VV_{jk}=WW_{jk}=0$ when j=k and $NN_{jk}=1$, the variance of the resonant displacement can be re-written as follows:

$$\begin{aligned}\sigma_{R,i}^2=\sum_{j=1}^{n}\sigma_{R,ji}^2\Bigg\{1+\sum_{\substack{k=1\\k\neq j}}^{n}\frac{\phi_{ik}}{\phi_{ij}}\Bigg[&NN_{jk}\frac{\int_{\omega_{j,s}}^{\omega_{j,e}}|H_j(i\omega)|^2\,\mathrm{Re}(S_{F_jF_k}(\omega))\,d\omega}{\int_{\omega_{j,s}}^{\omega_{j,e}}|H_j(i\omega)|^2S_{F_jF_j}(\omega)\,d\omega}\\&+PP_{jk}\frac{\int_{\omega_{j,s}}^{\omega_{j,e}}(1-\omega_j^2/\omega^2)|H_j(i\omega)|^2\,\mathrm{Re}(S_{F_jF_k}(\omega))\,d\omega}{\int_{\omega_{j,s}}^{\omega_{j,e}}|H_j(i\omega)|^2S_{F_jF_j}(\omega)\,d\omega}\\&+4VV_{jk}\frac{\int_{\omega_{j,s}}^{\omega_{j,e}}\left(\frac{\omega}{\omega_j}\right)|H_j(i\omega)|^2\,\mathrm{Im}(S_{F_jF_k}(\omega))\,d\omega}{\int_{\omega_{j,s}}^{\omega_{j,e}}|H_j(i\omega)|^2S_{F_jF_j}(\omega)\,d\omega}\\&+4WW_{jk}\frac{\int_{\omega_{j,s}}^{\omega_{j,e}}\left(\frac{\omega}{\omega_j}\right)^3|H_j(i\omega)|^2\mathrm{Im}(S_{F_jF_k}(\omega))\,d\omega}{\int_{\omega_{j,s}}^{\omega_{j,e}}|H_j(i\omega)|^2S_{F_jF_j}(\omega)\,d\omega}\Bigg]\Bigg\}\end{aligned} \tag{26}$$

For most of wind sensitive structures, the structural damping is usually very small, so $S_{F_jF_k}(\omega)$ could be regarded as a white noise excitation in the small integration interval of $[\omega_{j,s},\omega_{j,e}]$, i.e., $S_{F_jF_k}(\omega)=S_{F_jF_k}(\omega_j)=const$, where ω_j is the jth natural frequency of the structure. Moreover,

$$\frac{\omega_j^2}{\omega^2}=\frac{\omega}{\omega_j}=\left(\frac{\omega}{\omega_j}\right)^3\approx 1$$

for ω in the integration interval $[\omega_{j,s}, \omega_{j,e}]$, due to the very narrow frequency interval. Eq. (26) can thus be simplified as

$$\sigma_{R,i}^2 = \sum_{j=1}^{n} \sigma_{R,ji}^2 \left\{ 1 + \sum_{\substack{k=1 \\ k \neq j}}^{q} \frac{\phi_{ik}}{\phi_{ij}} \left[NN_{jk} \frac{\mathrm{Re}(S_{F_jF_k}(\omega_j))}{S_{F_jF_j}(\omega_j)} + 4(VV_{jk} + WW_{jk}) \frac{\mathrm{Im}(S_{F_jF_k}(\omega_j))}{S_{F_jF_j}(\omega_j)} \right] \right\} \tag{27}$$

Furthermore, letting $N_{jk} = NN_{jk}$ and $M_{jk} = 4(VV_{jk} + WW_{jk})$, one can re-write Eq. (27) as

$$\sigma_{R,i}^2 = \sum_{j=1}^{n} \sigma_{R,ji}^2 \left\{ 1 + \sum_{\substack{k=1 \\ k \neq j}}^{n} \frac{\phi_{ik}}{\phi_{ij}} \left[N_{jk} \frac{\mathrm{Re}(S_{F_jF_k}(\omega_j))}{S_{F_jF_j}(\omega_j)} + M_{jk} \frac{\mathrm{Im}(S_{F_jF_k}(\omega_j))}{S_{F_jF_j}(\omega_j)} \right] \right\} \tag{28}$$

Eq. (28) is the variance of resonant displacement with coupling effects of multi-modes. In Eq. (28), $\sigma_{R,ji}^2$ is the variance of the jth mode resonant displacement without mode coupling effects. Therefore, the term of

$$\sum_{\substack{k=1 \\ k \neq j}}^{n} \frac{\phi_{ik}}{\phi_{ij}} \left[N_{jk} \frac{\mathrm{Re}(S_{F_jF_k}(\omega_j))}{S_{F_jF_j}(\omega_j)} + M_{jk} \frac{\mathrm{Im}(S_{F_jF_k}(\omega_j))}{S_{F_jF_j}(\omega_j)} \right]$$

reflects the coupling effect between modes. N_{jk} and M_{jk} are both relative to the structural frequency and damping ratio, which will be further discussed later on.

2.2. Mode coupling factor and MSRSS method

To derive a simplified method for computation of resonant dynamic response with modal coupling of structures under the action of turbulent wind, Eq. (28) can be further written in the following simple style:

$$\sigma_{R,i}^2 = \sum_{j=1}^{n} \sigma_{R,ji}^2 (1 + \sum_{\substack{k=1 \\ k \neq j}}^{n} \theta_{jk}) = \sum_{j=1}^{n} \sigma_{R,ji}^2 (1 + \theta_j) \tag{29}$$

where

$$\theta_{jk} = \frac{\phi_{ik}}{\phi_{ij}} \left[N_{jk} \frac{\mathrm{Re}(S_{F_jF_k}(\omega_j))}{S_{F_jF_j}(\omega_j)} + M_{jk} \frac{\mathrm{Im}(S_{F_jF_k}(\omega_j))}{S_{F_jF_j}(\omega_j)} \right] \tag{30}$$

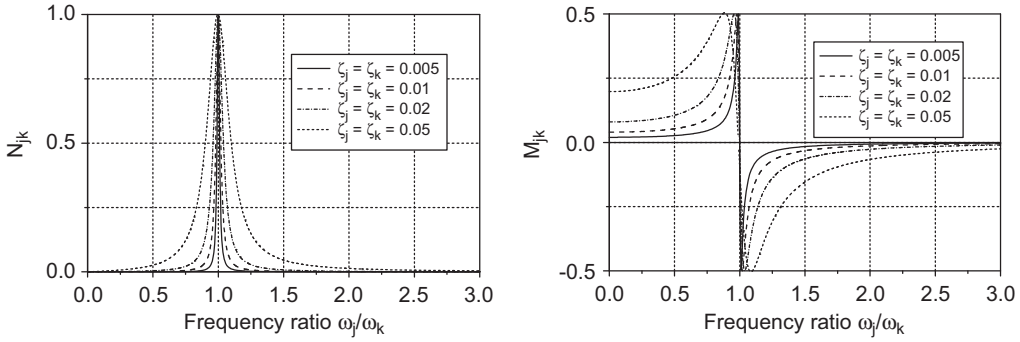

Fig. 1. Variations of N_{jk} and M_{jk} with frequency ratio ω_j/ω_k.

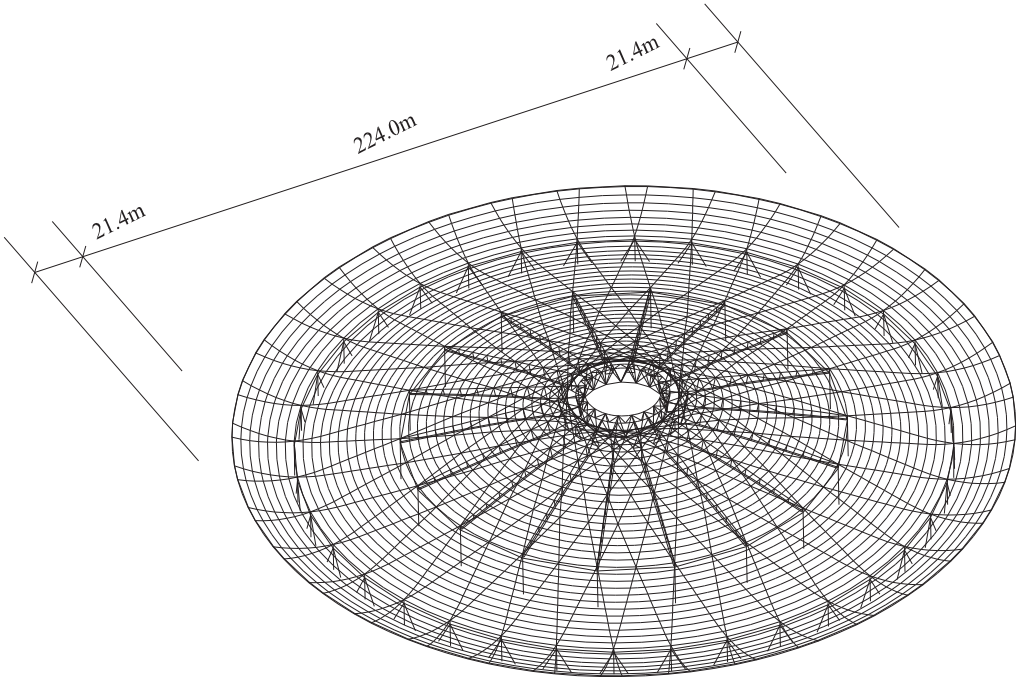

Fig. 2. Roof structure of Shanghai South Railway Station.

θ_{jk} is the modal coupling factor considering the kth modal coupling effect on the jth resonant response. Similarly,

$$\theta_j = \sum_{\substack{k=1 \\ k \neq j}}^{n} \theta_{jk}$$

is the jth modal coupling factor considering all the modal coupling effect on the jth resonant response.

The RMS value of the resonant displacement can thus be written as

$$\sigma_{R,i} = \sqrt{\sum_{j=1}^{n} \sigma_{R,ji}^2 (1+\theta_j)} \tag{31}$$

Eq. (31) is simple and convenient for computation of resonant dynamic responses of the structures with mode coupling effects under actions of turbulent wind. The present method is developed based on SRSS method and is called the modified SRSS method (MSRSS).

2.3. Analysis of N_{jk} and M_{jk}

N_{jk} and M_{jk} are the functions of structural damping ratios, ζ_j and ζ_k, and $q = \omega_j/\omega_k$, as mentioned above. Fig. 1 shows variation trends of N_{jk} and M_{jk} with structural frequency and damping. In the figure, N_{jk} varies with frequency in a narrow band fitter way with the peak at $\omega_j/\omega_k = 1$. The width of the curve of N_{jk} increases with the increase of structural damping ratio. For M_{jk}, when the frequency ratio ω_j/ω_k is smaller than unity, a positive peak can be found at $\omega_j/\omega_k = 1$; but when the frequency ratio is larger than unity, a negative peak appears also at $\omega_j/\omega_k = 1$. Similar to N_{jk}, the curve of M_{jk} is widened with the increase of the damping. Obviously, the structural damping and frequency have great influences on N_{jk} and M_{jk}. For the structures with small damping and well separated modal frequencies, N_{jk} and M_{jk} are both very small, indicating negligible coupling effects between modes.

3. Case study

To discuss the coupling effects between modes and to verify the precision of the MSRSS method for computation of buffeting responses with mode coupling of structures, a case study on Shanghai South Railway Station is made. The precise method, the SRSS method and the present MSRSS method are adopted in the computations. The so called precise method is the integration of Eq. (4) over the whole frequency range including all the concerned resonant frequencies but excluding the background component, as mentioned before.

The schematic diagram of roof structure of the Shanghai South Railway Station is shown in Fig. 2. The roof looks like a flat straw hat with an out-diameter of 270 m. It has a circular cantilever, the radial width of which is 21.4 m. The details of the structure, the wind tunnel test and the test results can be found in Gu et al. (2003) and only brief introductions are made.

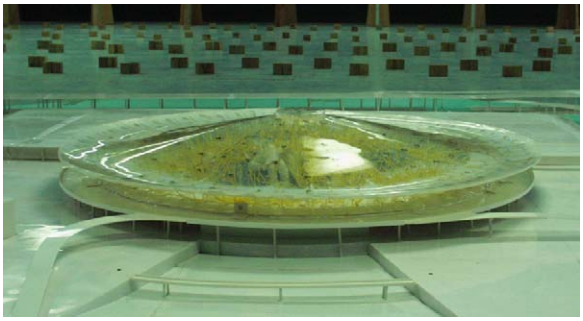

Fig. 3. Photograph of the roof model in wind tunnel.

3.1. Wind tunnel test and parameters for computation

In order to compute the dynamic responses of the roof, the fluctuating wind pressures acting on the roof were obtained from a wind tunnel test. The test was carried out in TJ-3 Boundary Layer Wind Tunnel in Tongji University, whose working section is 15 m wide and 2 m high. The geometry scale of the building model was 1:200, on which about 800 measuring points were arranged. The pressure taps were connected with the measurement system through PVC tubing. To avoid the distortion of the dynamic pressure, the signals had been modified using the transfer function of the tubing systems which had been developed by the authors. A DSM 3000 scan valve system was used to measure the wind pressures on the rigid model of the roof. The pressure signals were sampled at 300 Hz. Fig. 3 presents the photograph of the roof model in the wind tunnel.

According to the surrounding building situation around the Shanghai South Railway Station, the suburban field condition, corresponding to terrain category B defined in the Chinese code

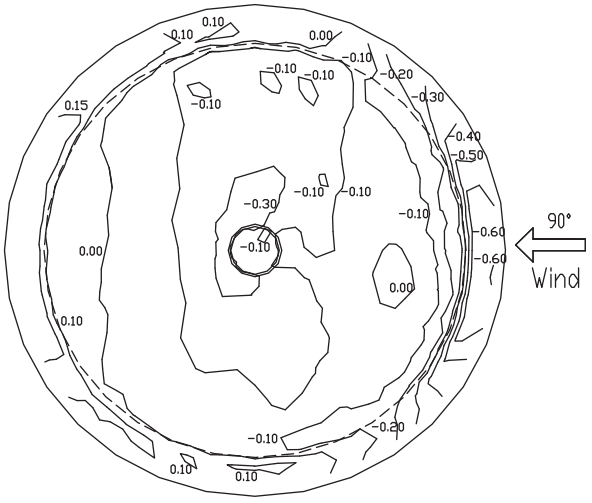

Fig. 4. Mean wind pressure coefficients on the roof.

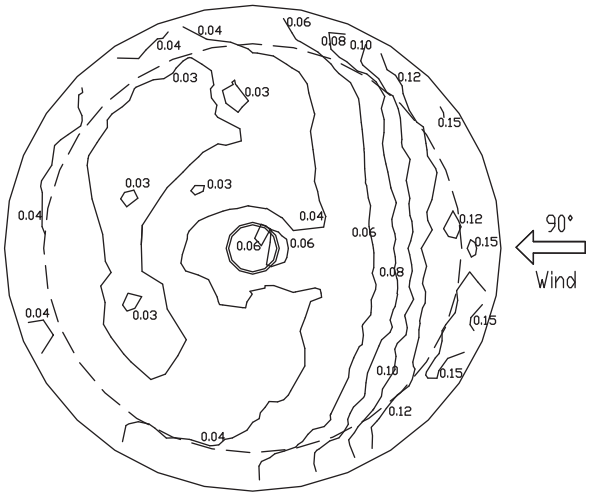

Fig. 5. RMS fluctuating wind pressure coefficients on the roof.

(GB 50009-2001), was simulated in the wind tunnel also at a length scale of 1:200 by a combination of turbulence generating spires and a barrier at the entrance of the wind tunnel, roughness elements along the wind tunnel floor upstream of the model. The exponent of the mean wind speed profile is 0.16, and the turbulent intensity is about 12% at the top of the building. The simulated turbulent intensity almost coincides with that defined in the Chinese code (GB 50009-2001), but seems smaller than that defined in codes of some other countries. However, effects of turbulence intensity on the dynamic responses of the building can be investigated under the present turbulence intensity to evaluate the applicability of the present method.

Figs. 4 and 5 show the typical mean pressure coefficients and RMS fluctuating wind pressure coefficients on the roof. Furthermore, the power spectrum densities and the coherences at the measuring points were obtained. These data are the base of the follow-up computation.

Furthermore, the dynamic behaviors of the building are computed before the computation of the wind induced responses. Fig. 6 presents some dominant mode shapes and the

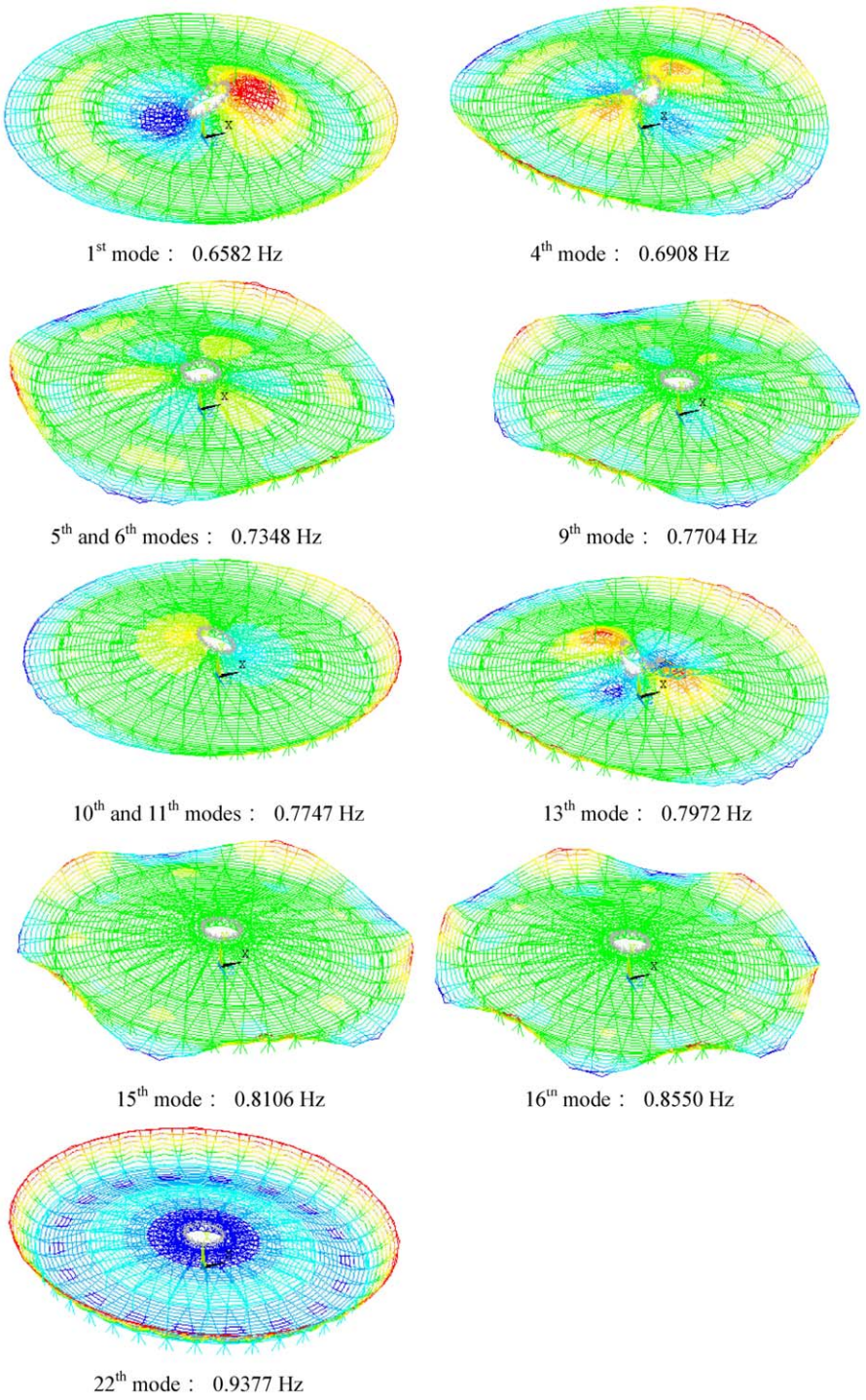

Fig. 6. Typical mode shapes and frequencies.

corresponding natural frequencies of the structure. From the detailed dynamic behaviors it can be found the building has a dense mode distribution, the first natural frequency being 0.6582 Hz and about 40 mode shapes ranging from 0.6582 to 1.1928 Hz.

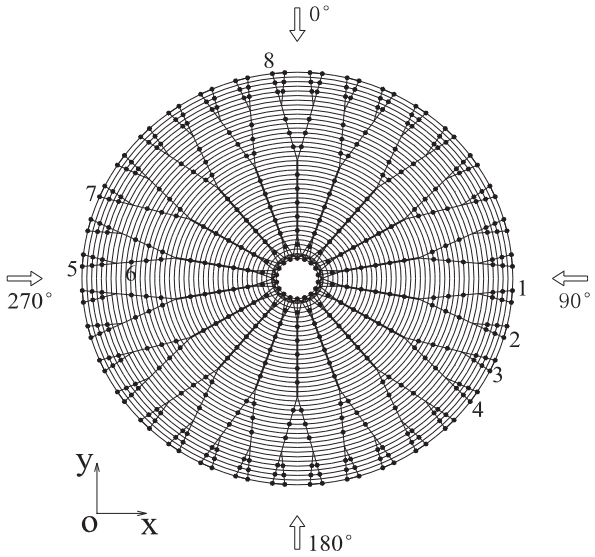

Fig. 7. Positions of selected points for computation.

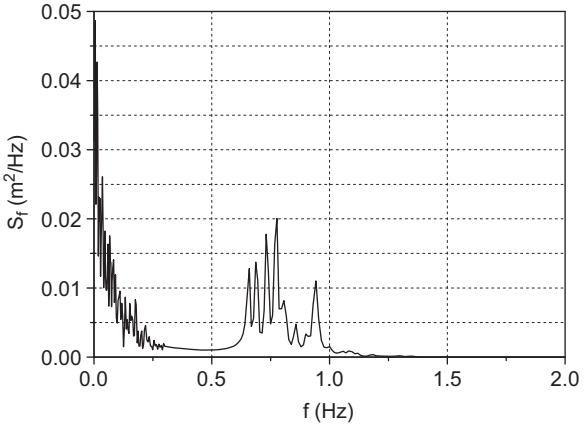

Fig. 8. Power spectrum of displacement at point 1.

The other wind parameters and structural parameters for the computation are: (1) 10 min averaged wind speed at 10 m height: 29.67 m/s; (2) the structural damping ratio: 0.01; (3) the number of modes participating in vibration: 50. The frequency range for the integration is $f \in [0.5, 2.500]$ Hz; the integration step $\Delta f = 0.0025$ Hz.

3.2. Computation results and comparison

With the above methods, the power spectra of dynamic displacements and the RMS values at some selected points (see Fig. 7) are computed. The power spectrum curve at the point 1, which is in the leading edge of the roof cantilever, is shown in Fig. 8. The displacement response at the point 1 is the largest compared with the other responses at the other selected points shown in Fig. 7. From the figure it can be seen that (1) the resonant response component plays a comparatively important role in the total resonant response; (2) the resonant frequencies are well separated from the background ones; (3) the contributions from the modes whose frequencies are higher than 2 Hz to the response are very small and so negligible. Therefore, the frequency range for the integration is $f \in [0.5, 2.5]$ Hz.

Table 1 lists the resonant displacements in different directions of the selected points 1–8, which are indicated in Fig. 7. In the table, the errors in bracket is defined as

$$(R_M - R_p)/R_P \times 100\% \tag{32}$$

where R_M is the RMS resonant displacement obtained using the SRSS method or the MSRSS method; R_P the RMS response from the precise method defined above. As can be seen from the table that the resonant displacements computed using the SRSS are around 10% larger or smaller than the precise values. These errors are believed to be caused by omitting the coupling effects between modes. While the MSRSS method is adopted, the computed responses are close to those computed with the precise method, with a maximum absolute error of −3.8% at the point 5.

Table 2 presents typical mode coupling factors of the resonant displacements at the point 1, which is in the leading edge of the roof cantilever (see Fig. 7), in z direction and the point 4 in x direction. The ratios of some important modal resonant displacement variances to the total resonant displacement variance, $\tilde{\sigma}^2_{R,ji}/\sigma^2_{R,i}$, are also listed in the table. In the table, the modes which have greater contributions to the resonant displacements at the points 1 and 4 are listed while those have contributions less than 3.4% and 3.3% to the resonant displacement variance for the points 1 and 4, respectively, are not presented. As can be seen from the table that the coupling

Table 1
Comparison of the resonant responses from methods.

Computation methods	RMS of resonant displacements (error)			
	Point 1 (z–D)	Point 2 (x–D)	Point 3 (z–D)	Point 4 (x–D)
"Precise" method	51.4 (0.0%)	13.6 (0.0%)	55.4 (0.0%)	12.5 (0.0%)
SRSS	47.3 (−8.2%)	12.3 (−9.5%)	50.7 (−8.5%)	11.1 (−11.3%)
MSRSS	53.0 (2.9%)	14.0 (2.9%)	57.4 (3.6%)	12.9 (2.7%)
Computation methods	RMS of resonant displacements (error)			
	Point 5 (z–D)	Point 6 (y–D)	Point 7 (y–D)	Point 8 (x–D)
"Precise" method	47.3 (0.0%)	2.1 (0.0%)	6.8 (0.0%)	7.1 (0.0%)
SRSS	51.6 (9.3%)	2.3 (11.3%)	7.4 (9.3%)	6.5 (−8.5%)
MSRSS	45.4 (−3.8%)	2.0 (−3.3%)	6.6 (−3.0%)	7.0 (−1.3%)

Note: 1. Number in brackets is errors; 2. unit of displacement is mm.

Table 2
Modal coupling factors of some typical nodes.

Point 1 (z-direct.)	Mode number	1	4	5	6	10	11	13	15	16	22
	θ_j	0.24	0.20	0.09	−0.16	0.27	0.94	0.53	0.36	0.19	0.02
	$\tilde{\sigma}^2_{R,ji}/\sigma^2_{R,i}$ (%)	9.5	13.2	14.2	3.4	9.0	16.0	3.4	6.6	4.6	11.4
Point 4 (x-direct.)	Mode number	1	4	5	6	9	10	11	13	14	16
	θ_j	0.33	0.25	0.39	0.31	0.77	0.44	0.45	0.45	0.63	0.22
	$\tilde{\sigma}^2_{R,ji}/\sigma^2_{R,i}$ (%)	4.3	8.0	7.6	10.4	10.0	22.4	4.4	8.7	3.3	3.5

factors can make positive or negative influences on the response, i.e., increasing or decreasing the resonant response. $\theta_{11}=0.94$ at the point 1 means the coupling effects between the 11th mode and the other modes can make a 48.5% (0.94/[1+0.94]=48.5%) contribution to the 11th mode resonant displacement variance; or in other words, if the 11th mode coupling effect was neglected, the 11th mode resonant displacement variance would be about half of the actual one. On the contrary, the 6th mode coupling with the other modes will make a negative effect ($\theta_6=-0.16$) on the resonant response. Moreover, $\tilde{\sigma}^2_{R,11i}/\sigma^2_{R,i}=16\%$ means that the 11th resonant displacement variance makes a 16% contribution to the total response variance. Compared with the other modal values of $\tilde{\sigma}^2_{R,ji}/\sigma^2_{R,i}$, one can also see that the 11th mode has a greatest contribution to the total resonant displacement variance. Similarly, for the point 4, the response components of the modes 6, 9 and 10 have the main contributions to the total resonant displacement, in which the 10th resonant displacement variance makes a 22.4% contribution to the total resonant response variance. Moreover, the coupling effects between the 10th mode and the other modes can make a 30.6% (0.44/[1+0.44]=30.6%) contribution to the 10 mode resonant displacement variance; while the 10th resonant displacement variance makes a 22.4% contribution to the total resonant response variance.

4. Concluding remarks

The new cencept of "mode coupling factor" describing the coupling effects between multi-mode resonant responses, and accordingly the modified SRSS mthod for computation the dynamic resonant response of flexible structures with concentrated modes and low damping are proposed in the paper. The mode coupling factor could quantitatively describe the contribution of mode coupling to the resonant response; and the modified SRSS method could make the computation of resonant response with mode coupling effects of the structures much simpler. The roof structure of Shanghai Southern Railway Station is then taken as the case study to indicate the application and to verify the precision of the mode coupling factor and the modified SRSS method. The computed results indicate that the coupling effects between modes of the specific structure are significant and can be quantitatively described by the mode coupling factor. Moreover, the computed resonant displacements of the roof structure using the MSRSS method agree well with the precise solutions.

Acknowledgments

This project is jointly supported by National Natural Science Foundation (50621062, 90715040, 50608060) and National Science and Technology R&D Program in the 11th Five-Year Plan of China (2006BAJ06B05), which are gratefully acknowledged.

References

Davenport, A.G., 1995. How can we simplify and generalize wind loads. Journal of Wind Engineering and Industrial Aerodynamics 54/55, 657–669.
Gu, M., Huang, P., Zhu, C.H., 2002. Wind resistant research on wind loads and responses of Putian stadium. Research Report, State Key Laboratory for Disaster Reduction in Civil Engineering, Tongji University (in Chinese).
Gu, M., Zhou, X.Y., Huang, P., 2003. Wind resistant research on wind loads and responses of Shanghai Southern Railway Station. Research Report, State Key Laboratory for Disaster Reduction in Civil Engineering, Tongji University (in Chinese).
Holmes, J.D., 1999. Equivalent static load distributions for resonant dynamic response of bridges. In: Proceedings of the 10th International Conference on Wind Engineering, Copenhagen, Balkema, pp. 907–911.
Holmes, J.D., 2002. Effective static load distributions in wind engineering. Journal of Wind Engineering and Industrial Aerodynamics 90 (2), 91–109.
Holmes, J.D., Kasperski, M., 1996. Effective distributions of fluctuating and dynamic wind load. Australian Civil/Structural Engineering Transactions CE 38, 83–88.
Kasperski, M., Niemann, H.J., 1992. The L.R.C. (load-response-correlation)-method: a general method of estimating unfavorable wind load distributions for linear and non-linear structural behavior. Journal of Wind Engineering and Industrial Aerodynamics 43 (1–3), 1753–1763.
Load code for the design of building structure (GB 50009-2001), 2006. China Architecture & Building Press.
Nakamura, O., Tamura, Y., Miyashita, K., Itoh, M., 1994. A case study of wind pressure and wind-induced vibration of a large span open-type roof. Journal of Wind Engineering and Industrial Aerodynamics 52, 237–248.
Simu, E., Scanlan, R.H., 1996. Wind Effects on Structures, third ed Wiley, New York.
Uematsu, Y., Kuribara, O., Yamada, M., Sasakic, A., Hongo, T., 2001. Wind-induced dynamic behavior and its load estimation of a single-layer latticed dome with a long span. Journal of Wind Engineering and Industrial Aerodynamics 89 (14–15), 1671–1687.
Uematsu, Y., Watanabe, K., Sasaki, A., Yamada, M., Hongo, T., 1999. Wind-induced dynamic response and resultant load estimation of a circular flat roof. Journal of Wind Engineering and Industrial Aerodynamics 83 (1–3), 251–261.
Vanmarcke, E.H., 1972. Properties of spectral moments with applications to random vibration. Journal of Engineering Mechanics Division, ASCE 98, 425–446.
Zhou, Y., Gu, M., Xiang, H.F., 1999. Along-wind static equivalent wind loads and responses of tall buildings. Part I: unfavorable distributions of static equivalent wind loads. Journal of Wind Engineering and Industrial Aerodynamics 79 (1–2), 135–150.
Zhou, Y., Kareem, A., Gu, M., 2000. Equivalent static buffeting wind loads on structures. Journal of Structural Engineering, ASCE 126, 989–992.